

An approach to retrieve information on the carbonyl fluoride (COF₂) vertical distributions above Jungfraujoch by FTIR multi-spectrum multi-window fitting

P. Duchatelet¹, E. Mahieu¹, R. Ruhnke², W. Feng³, M. Chipperfield³, P. Demoulin¹, P. Bernath^{4,5}, C. D. Boone⁵, K. A. Walker^{5,6}, C. Servais¹, and O. Flock¹

¹Institute of Astrophysics and Geophysics of the University of Liège, B-4000 Liège, Belgium

²Forschungszentrum Karlsruhe, IMK, Karlsruhe, Germany

³Institute for Climate and Atmospheric Science, School of Earth and Environment, University of Leeds, Leeds, UK

⁴Department of Chemistry, University of York, Heslington, UK

⁵Department of Chemistry, University of Waterloo, Waterloo, Canada

⁶Department of Physics, University of Toronto, Toronto, Canada

Received: 7 October 2008 – Published in Atmos. Chem. Phys. Discuss.: 30 January 2009

Revised: 8 October 2009 – Accepted: 8 October 2009 – Published: 30 November 2009

Abstract. We present an original multi-spectrum fitting procedure to retrieve volume mixing ratio (VMR) profiles of carbonyl fluoride (COF₂) from ground-based high resolution Fourier transform infrared (FTIR) solar spectra. The multi-spectrum approach consists of simultaneously combining, during the retrievals, all spectra recorded consecutively during the same day and with the same resolution. Solar observations analyzed in this study with the SFIT-2 v3.91 fitting algorithm correspond to more than 2900 spectra recorded between January 2000 and December 2007 at high zenith angles, with a Fourier Transform Spectrometer operated at the high-altitude International Scientific Station of the Jungfraujoch (ISSJ, 46.5° N latitude, 8.0° E longitude, 3580 m altitude), Switzerland. The goal of the retrieval strategy described here is to provide information about the vertical distribution of carbonyl fluoride. The microwindows used are located in the ν_1 or in the ν_4 COF₂ infrared (IR) absorption bands. Averaging kernel and eigenvector analysis indicates that our FTIR retrieval is sensitive to COF₂ inversion between 17 and 30 km, with the major contribution to the retrieved information always coming from the measurement. Moreover, there was no significant bias between COF₂ partial columns, total columns or VMR profiles retrieved from the two bands. For each wavenumber region, a complete error budget including all identified sources has

been carefully established. In addition, comparisons of FTIR COF₂ 17–30 km partial columns with KASIMA and SLIMCAT 3-D CTMs are also presented. If we do not notice any significant bias between FTIR and SLIMCAT time series, KASIMA COF₂ 17–30 km partial columns are lower of around 25%, probably due to incorrect lower boundary conditions. For each time series, linear trend estimation for the 2000–2007 time period as well as a seasonal variation study are also performed and critically discussed. For FTIR and KASIMA time series, very low COF₂ growth rates ($0.4 \pm 0.2\%/year$ and $0.3 \pm 0.2\%/year$, respectively) have been derived. However, the SLIMCAT data set gives a slight negative trend ($-0.5 \pm 0.2\%/year$), probably ascribable to discontinuities in the meteorological data used by this model. We further demonstrate that all time series are able to reproduce the COF₂ seasonal cycle, which main seasonal characteristics deduced from each data set agree quite well.

1 Introduction

Over the past few decades, the major sources of fluorine in the stratosphere are the man-made chlorofluorocarbons CFC-12 (CCl₂F₂) and CFC-11 (CCl₃F), which have been widely emitted at ground level by human activities. Photolysis of these compounds leads to release of chlorine atoms, while the fluorine is, for the first steps, present in the form of carbonyl compounds like carbonyl chlorofluoride (COCIF) and



Correspondence to: P. Duchatelet
(p.duchatelet@ulg.ac.be)

carbonyl fluoride (COF₂). These two species are long-lived enough to be detectable from the ground (Mélen et al., 1998) or by in situ techniques (Wilson et al., 1989) and their photolysis further liberates fluorine atoms, which are quickly converted to HF. Its extreme stability makes HF the largest fluorine reservoir in the stratosphere, but COF₂ also makes a large contribution to the inorganic fluorine budget F_y , because of its slow photolysis (Sen et al., 1996): the COF₂ molecule has been shown to be the second most abundant stratospheric fluorine reservoir (Kaye et al., 1991). The maximum contribution of COF₂ to F_y is in the tropics, where it accounts for about 32% at its peak altitude near 40 km (Nassar et al., 2006). At midlatitudes, the COF₂ vertical distribution has a maximum around 30 km where it contributes to almost 25% to F_y (Nassar et al., 2006). Despite the fact that fluorine does not directly participate in ozone depletion, measurement of the concentrations of individual fluorine-bearing species in different altitude ranges of the atmosphere is important: (1) to quantify the strengths of the various sources and to compare with emission inventories, (2) to assess their partitioning during the transformation from sources to sink species.

Measurements of COF₂ are however still sparse. Rinsland et al. (1986) were the first to detect COF₂ in the Earth's stratosphere and to produce a carbonyl fluoride vertical profile obtained from ATMOS/Spacelab 3 space observations using line parameters derived from laboratory spectra. These observations were in good agreement with model predictions published by Kaye et al. (1991). In addition, a comparison between mean COF₂ vertical distributions for different latitudinal regions recorded in 1985 and 1992 during the ATMOS/Spacelab 3 and ATMOS/Atlas 1 space missions, respectively, has been discussed by Zander et al. (1994). The Atmospheric Chemistry Experiment Fourier transform spectrometer (ACE-FTS), onboard the SCISAT-1 satellite, is the first instrument since the last ATMOS flight in 1994 to obtain COF₂ vertical profiles from space (Bernath et al., 2005). Launched in August 2003, the ACE-FTS has been regularly taking COF₂ measurements with global coverage since early 2004. A paper by Walker et al. (2009) will exploit the v.3 of the ACE-FTS data to study the global distribution of carbonyl fluoride.

Several COF₂ IR absorption lines can also be used to determine its total column from ground-based Fourier transform infrared (FTIR) observations. In this context, different studies concerning the measurement of the COF₂ total column above various sites were published during the nineties: Rinsland et al. (1991) were the first to report a mean COF₂ total column measured above Kitt Peak (31.9° N latitude, 111.6° W longitude, 2090 m altitude) and to confront their results with calculations made by the two dimensional Atmospheric and Environmental Research (AER) model (Ko et al., 1989). A subsequent paper by Reisinger et al. (1994) proposed innovative COF₂ measurements using the ν_4 absorption features at 1234 cm⁻¹. Independently Notholt et

al. (1995) have exploited a pair of COF₂ microwindows located either in the ν_1 (1935 and 1950 cm⁻¹ regions) or the ν_4 (1235 cm⁻¹ region) band to publish total column values measured at high northern latitude during summer 1993 and 1994. No significant bias between the two time series was found. The first contribution dealing with the full characterization of the seasonal variability and the global trend of carbonyl fluoride is a paper by Mélen et al. (1998). These authors have exploited two microwindows located in the ν_1 band to produce a time series covering the 1985–1995 time period from solar spectra recorded at the Jungfraujoch. One year later, Mélen et al. (1999) compared COF₂ total columns above Jungfraujoch derived from the ν_1 and the ν_4 bands and found a bias of 6%, with the ν_4 band results being lower than those derived from the ν_1 band. In addition, no information on the COF₂ vertical distribution could be retrieved following any of the studies described above.

To our knowledge, no study about the inversion of COF₂ vertical distributions from ground-based FTIR spectra has been published to date. This study deals with the possibility of such inversions using, simultaneously, a multi-microwindow and a multi-spectrum fitting procedure. A selection of microwindows in the so-called InSb (2–5.5 μm , including the ν_1 COF₂ band) and MCT (7–14 μm , including the ν_4 COF₂ band) spectral ranges, a complete discussion of the data characterization (e.g. information content and error budget) and typical examples of COF₂ retrieved products from ground-based FTIR spectra are presented here. Comparisons with KASIMA and SLIMCAT model data are also included.

2 Retrieval strategy

All the results produced in this study have been derived from high resolution solar spectra recorded at the International Scientific Station of the Jungfraujoch (ISSJ, Swiss Alps; 46.5° N latitude, 8.0° E longitude, 3580 m altitude) under clear-sky conditions with a commercial Bruker IFS 120HR spectrometer between January 2000 and December 2007. For the present work, two sets of spectral microwindows have been defined and selected in the ν_1 and the ν_4 COF₂ absorption bands. Table 1 summarizes the main characteristics of each set. Since COF₂ absorption lines are quite weak, only spectra with solar zenith angles greater than 70° and up to 90° have been analyzed. Spectral resolutions, defined as the inverse of twice the maximum optical path difference, are 2.85 and 4.40 millicm⁻¹ for the InSb set, and 4.00 and 6.10 millicm⁻¹ for the MCT microwindows. For each detector band, two different spectral resolutions are used, pending of the time of measurements (low or high sun in the sky) and weather conditions (clear or partly cloudy conditions).

The COF₂ column retrievals and profile inversions have been performed using the SFIT-2 v3.91 fitting algorithm. This retrieval code has been specifically developed to derive

volume mixing ratio (VMR) profiles of atmospheric species from ground-based FTIR spectra. Inversion of vertical distributions from infrared measurements is often an ill-conditioned problem. Regularization methods are therefore frequently used to improve the conditioning of the solution (Ceccherini, 2005). The SFIT-2 algorithm employs a semi-empirical implementation of the Optimal Estimation Method (OEM) developed by Rodgers (2000), as well as error evaluation as discussed in Connor et al. (1995). The OEM is a regularization method that retrieves VMR profiles from a statistical weighting of a priori information and the measurements. The weighting matrix (called the averaging kernel, **AvK**) produced during the iterative process can be further used to characterize the information content of the retrievals. A more complete description of the SFIT-2 code can be found, for example, in Pougatchev and Rinsland (1995), Pougatchev et al. (1995) and Rinsland et al. (1998). During our retrievals, only the COF₂ vertical distribution has been fitted, while the a priori VMR profiles corresponding to interfering species were simply scaled. The synthetic spectra were calculated with the spectroscopic line parameters available in the latest 2004 version of the HITRAN compilation (Rothman et al., 2005). During the retrievals, all microwindows of each set were fitted simultaneously. In addition, we have also performed multi-spectrum retrievals during which several FTIR spectra, recorded during the same day at identical resolutions and similar solar zenith angles, are fitted together to increase the information content (see Sect. 3). However, for the InSb set, spectra recorded during the morning and during the afternoon have to be retrieved separately, due to the high variability of water vapor, a significant interference in the 1936 cm⁻¹ microwindow. During this multi-spectrum multi-window fitting procedure, individual air mass files are also computed for each spectrum. Between 15 and 37 km, the adopted a priori COF₂ profile is a zonal mean (for the 41–51° N latitude band) of more than 300 occultations recorded by the ACE-FTS instrument between February 2004 and September 2005. The ACE-FTS COF₂ profiles used in this study consist in a research version of ACE-FTS v.2.2 products. They differ from the standard 2.2 version by higher retrieval heights for COF₂. Below 15 km, ACE-FTS VMR values have been smoothly connected to reach VMR values of about 1.5×10^{-13} at the altitude of the site (3.58 km), which corresponds to the COF₂ ground value used by Mélen et al. (1998). Above 37 km (this altitude corresponds to the highest ACE-FTS analyzed measurement), the a priori COF₂ profile used by ACE-FTS is scaled during its retrieval procedure. These scaled profiles (once again, for all ACE-FTS occultations located in the 41–51° N latitude band) have then been averaged in order to construct our own a priori COF₂ profile above 37 km. The a priori covariance matrix **S_a** has been derived from the same set of ACE-FTS measurements used for the construction of the a priori COF₂ profile. Each diagonal element of the **S_a** matrix has also been weighted by the square root of the corresponding atmospheric layer thickness, to account for vari-

Table 1. Microwindows selected (in InSb and MCT ranges) for COF₂ profile inversions. Second column lists the interfering gases adjusted during the retrieval process. For each microwindow, examples of simulated spectra (for a solar angle close to 80°) with the contribution of COF₂ are reproduced on Fig. 3.

Range (cm ⁻¹)	Interfering species
InSb range (2–5.5 μm)	
1936.15–1936.34	O ₃ , CO ₂ , H ₂ O, solar lines
1951.89–1952.05	O ₃ , H ₂ O, solar lines
1952.62–1952.78	O ₃ , CO ₂ , solar lines
MCT range (7–14 μm)	
1230.75–1231.20	CH ₄ , O ₃ , CO ₂ , H ₂ O ₂ , N ₂ O
1233.90–1234.20	CH ₄ , O ₃ , CO ₂ , H ₂ O ₂ , N ₂ O, solar lines
1234.35–1234.63	CH ₄ , O ₃ , CO ₂ , H ₂ O ₂ , N ₂ O, CH ₃ D

able layer thicknesses. A Gaussian inter-layer correlation of 2 km has further been implemented, estimated from the 3D VMR-altitude correlation matrix, as calculated from the ACE-FTS observations. Top panel of Fig. 1 illustrates the COF₂ a priori VMR and variability profiles (this latter one corresponding to diagonal elements of the **S_a** matrix) used for our retrievals. Background horizontal lines reproduce the 41 atmospheric layer scheme used during the retrieval procedure. The COF₂ VMR-altitude correlation matrix as seen by the ACE-FTS instrument and from which the correlation length parameter has been deduced is illustrated on the bottom panel of Fig. 1. The adopted pressure–temperature (*p*–*T*) profiles were those provided by the National Centers for Environmental Prediction (NCEP, Washington, DC.; see <http://www.ncep.noaa.gov>), specifically computed for the Jungfraujoch site on a daily basis. The signal-to-noise ratio used during the retrievals and allowing to define diagonal elements of the diagonal measurement covariance matrix **S_e** was fixed to 250, following the L-curve method (for example, Steck, 2002; Ceccherini, 2005).

3 Information content and error budget

Under the input and observational conditions described here above, each microwindow set has been completely characterized in terms of information content. Table 2 objectively demonstrates the benefits of using, simultaneously, a multi-microwindow (MW) and a multi-spectrum (MS) approach for COF₂ retrievals. The last column of Table 2 provides, for each selected microwindow, typical values for the degrees of freedom for signal (DOFS) when the retrieval is done using this single microwindow alone: this parameter indicates how many independent pieces of information of the target gas distribution (computed here for partial columns) may be

Table 2. Typical information content of microwindows sets selected for COF₂ profile inversions. Second column gives the degrees of freedom for signal (DOFS) and the fraction of information coming from the measurement (λ_1) when each interval is fitted separately. Lines “3MW” and “3MW+MS_[3obs]” indicate the DOFS and λ_1 when a multi-microwindow (including the 3 microwindows of the previous lines) and a multi-microwindow multi-spectrum (including 3 FTIR observations) fitting procedure is adopted, respectively. Solar zenith angles of the spectra used for these simulations are close to 78°.

Range (cm ⁻¹)	DOFS (λ_1)
InSb range (2–5.5 μm)	
1936.15–1936.34	0.53 (0.49)
1951.89–1952.05	0.58 (0.53)
1952.62–1952.78	0.60 (0.54)
3MW	0.94 (0.53)
3MW+MS _[3obs]	1.24 (0.92)
MCT range (7–14 μm)	
1230.75–1231.20	0.37 (0.35)
1233.90–1234.20	0.35 (0.33)
1234.35–1234.63	0.35 (0.33)
3MW	0.68 (0.63)
3MW+MS _[3obs]	0.95 (0.81)

derived. Values between brackets (λ_1) correspond to the first eigenvalue of the corresponding $\mathbf{A}\mathbf{v}\mathbf{K}$ matrix and indicate the fraction of the information coming from the measurement.

The line “3MW” gives the DOFS and λ_1 resulting when all microwindows are fitted simultaneously. In the InSb case, a multi-microwindow fit provides a significant increase in the DOFS, but has a minor impact on the first eigenvalue. Only a multi-spectrum fitting procedure allows a larger fraction of the information to come from the measurement (see line “3MW+MS_[3obs]” in Table 2; values reported are from the inclusion of 3 spectra). For the MCT range, a multi-microwindow fit doubles the DOFS and the λ_1 value compared to the single MW fits and an even larger improvement is obtained by applying the multi-spectrum approach. It is therefore possible to compute one COF₂ partial column (DOFS greater or close to 1) when such a multi-spectrum procedure is adopted, with very limited impact from the adopted a priori.

More complete statistics have been established by analyzing FTIR spectra recorded at the Jungfraujoch during the January 2000–December 2007 time period. For the solar zenith angle range adopted here, our database contains 884 spectra recorded over 252 days for the InSb domain, and 2062 FTIR observations recorded over 439 days for the MCT range. Corresponding mean DOFS values are 1.23 ± 0.17 and 1.16 ± 0.30 for the InSb and MCT regions, respectively. For the InSb range, the minimum value of 0.88 for the DOFS

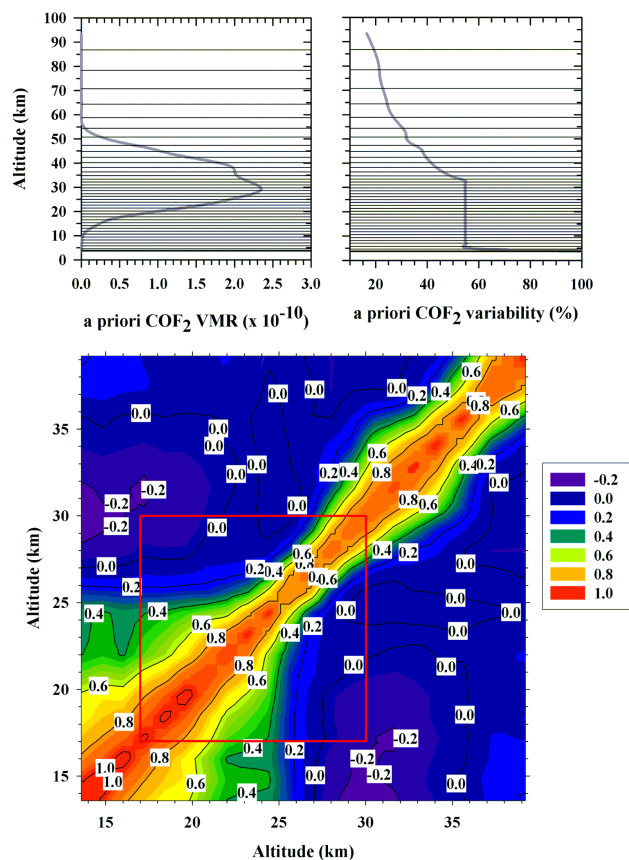


Fig. 1. Top panel: a priori VMR (left) and variability (right) profiles used for our COF₂ profile inversions. Horizontal lines reproduce the 41 atmospheric layers used during the retrieval procedure. Bottom panel: COF₂ VMR – altitude correlation matrix as deduced from ACE-FTS satellite mid-latitude observations (41–51° N). The red square indicates the altitude range where FTIR retrievals are sensitive to COF₂ inversion. Outside these ranges, the COF₂ variability mainly results from the ACE-FTS a priori information.

is observed when combining 2 spectra and the maximum value of 2.07 is obtained by fitting 8 spectra simultaneously. Corresponding λ_1 are 0.76 and 0.99, respectively. For the MCT case, the minimum value of the DOFS is 0.60 for 2 FTIR spectra fitted simultaneously, while the maximum value peaks at 1.95 for the combination of 15 spectra in the retrievals. Corresponding λ_1 values are 0.56 and 0.99, respectively. It thus clearly appears that, for the same number of FTIR spectra combined during the retrieval procedure, the COF₂ lines selected in the ν_1 band provide more information than the COF₂ absorptions selected in the ν_4 region. Among the factors explaining why the InSb microwindows bring higher information content, are: (1) the weakness of COF₂ absorption lines in the MCT region as compared to the lines selected in the InSb range (InSb COF₂ lines are stronger by almost a factor 2) and, (2) the higher spectral resolution of the ISSJ observations performed in the InSb region

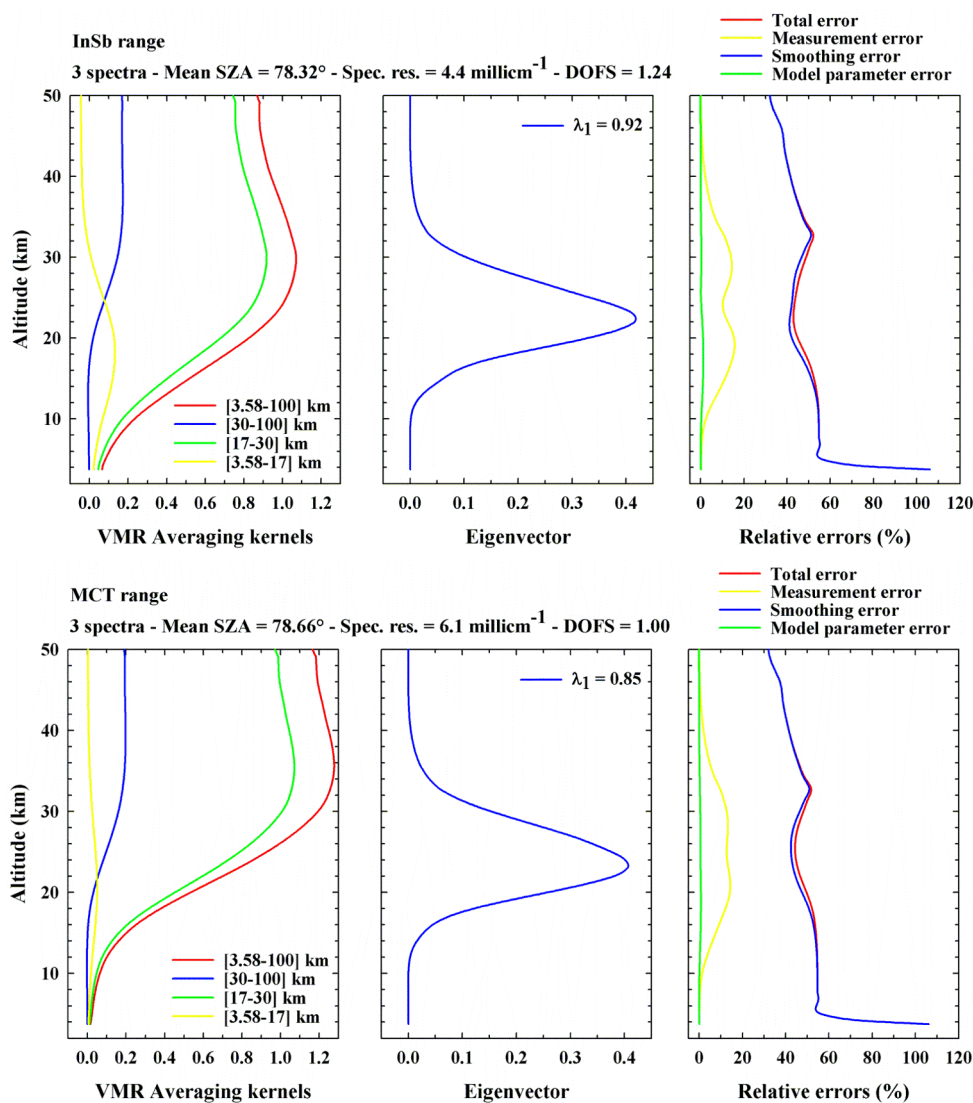


Fig. 2. Typical information content for COF₂ retrievals from ISSJ spectra using the InSb (top panel) and the MCT (lower panel) regions. For each spectral range, these curves have been calculated by applying simultaneously the multi-microwindow and multi-spectra fitting procedure on 3 FTIR spectra recorded at high and similar mean solar zenith angles, on 30 January 2006 for the InSb range, on 8 March 2002 for the MCT range.

(as already mentioned in Sect. 2). For the time period under investigation here, three spectra can be combined in almost 80% of cases for the InSb region, and in 48% of cases for the MCT range. In both spectral domains, the fraction of occurrences for which spectra are combined only in pairs never exceeds 12%.

For typical VMR averaging kernels, the first eigenvector of the **AvK** matrix and partial error budgets are plotted in the top panel of Fig. 2 for the InSb range, in its lower panel for the MCT region. All these curves have been simulated by using 3 FTIR spectra in the multi-microwindow multi-spectra fitting procedure, as defined in Table 2. The observational conditions (including the resolutions) used for the

simulation are indicated above each panel. Averaging kernels have been calculated for the altitude ranges defined in the legend. They indicate a good sensitivity of the ground-based FTIR observations for COF₂ retrievals between 17 and 50 km. Outside of this altitude range, the sensitivity to the measurement is quite poor. However, the half-width at half-maximum of the first eigenvector curve (middle frame) suggests that FTIR measurements are mostly sensitive between 17 and 30 km, with the maximum sensitivity observed around 25 km. Corresponding first eigenvalues indicate that in both spectral ranges, the largest fraction of the information is coming from the measurement (contributions of 92% and 85% for the InSb and MCT domains, respectively). The

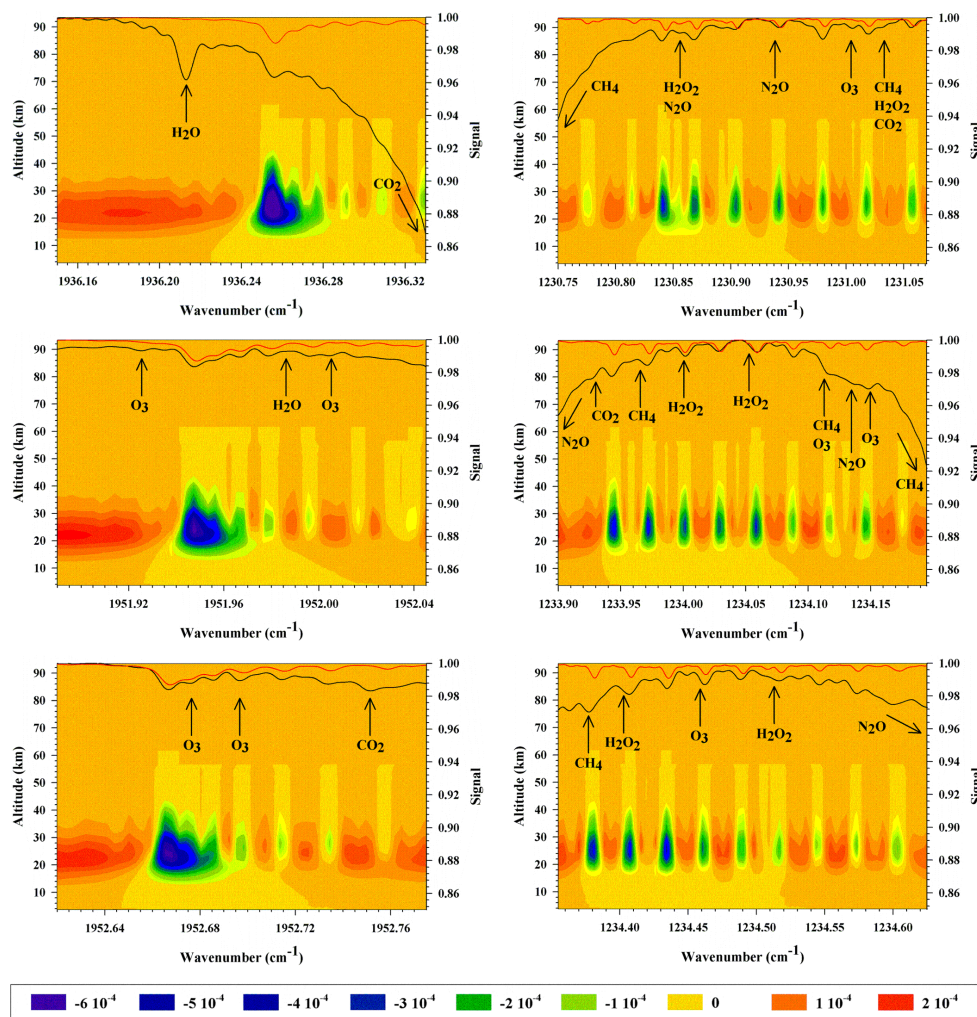


Fig. 3. Selection of microwindows in InSb (left column) and MCT (right column) ranges for COF₂ profile inversions. For each microwindow, black and red traces (slightly vertically scaled, for clarity) reproduce all gases and COF₂ absorptions, respectively (simulated spectra performed for a solar zenith angle of 80°). All atmospheric interference gases for which VMR profiles are scaled during the retrieval procedure are indicated with black arrows (minor interferences due to solar lines are not represented for clarity). Background colored plots reproduce, for each microwindow, corresponding typical **K** matrix weighting functions and highlight the altitude sensitivity range of each COF₂ absorption line.

value of the DOFS obtained in each case (1.24 and 1.00, as mentioned in the legend of Fig. 2) indicates that one partial column can be extracted from COF₂ FTIR measurements, when performing a retrieval using the multi-microwindow multi-spectrum approach. The altitude limits of such a partial column could be, for example, the ones we have chosen to plot the non zero averaging kernels illustrated on the left part of Fig. 2, i.e., 17–30 km. Another way to highlight the altitude sensitivity range of our set of COF₂ absorption lines is to plot the **K** matrix weighting function characterizing our COF₂ vertical profile inversions. A typical example of a **K** matrix for the COF₂ retrieval using the multi-microwindow multi-spectrum approach is reproduced on the background colored plots of Fig. 3. For each microwindow of our set (left

column: InSb range; right column: MCT range) black and red traces (slightly vertically scaled, for clarity) reproduce all gases and COF₂ absorption contributions, respectively. These traces correspond to simulated spectra performed for a solar zenith angle close to 80°. Significant interference gases for which VMR profiles are scaled during the retrieval procedure are also labeled with black arrows. It clearly appears from Fig. 3 that our FTIR measurements using the multi-microwindow multi-spectrum approach are most sensitive to COF₂ inversions between 17 and 30 km.

Finally, a typical example of the error budget for the retrieved COF₂ VMR profiles is given in the right frames of Fig. 2. Only contributions to the total error of the three most common random error components (namely, smoothing

error, measurement error and forward model parameter error) are plotted; for the InSb range, these together correspond typically to 8% and 11% of the COF₂ total and 17–30 km partial columns, respectively. Due to lower information content and spectral resolution, the corresponding errors for the MCT range are a little higher, with typical values for total error of 11% and 15%, respectively. The S_a matrix used for the estimation of smoothing error is the variability matrix deduced from ACE-FTS satellite data (see end of Sect. 2). The forward model parameter error includes errors induced by retrieval parameters (like, e.g., the wavenumber shift, the background slope, the background curvature, etc) which can improve fitting quality when they are adjusted during the retrieval procedure. In our case, only the wavenumber shift and the background slope are adjusted during the retrieval procedure, for each microwindow of both spectral regions (InSb and MCT). An independent wavenumber shift for each microwindow is also applied. When a microwindow contains solar absorption lines, the error induced by the solar line shift is also included in the forward model parameter error. Three additional random error sources, namely errors associated with the temperature profiles used in the physical model adopted for the retrievals, with the instrument line shape (ILS) and with the solar zenith angle (SZA), have also been evaluated by using a perturbation method. To quantify the effect of temperature profile errors on COF₂ total and partial columns, we have included the temperature uncertainties provided by the NCEP in our retrieval procedure. The ILS error has been evaluated by assuming an effective apodization error of $\pm 10\%$, compared to a perfectly aligned instrument. For the time period studied here, this $\pm 10\%$ value is consistent with the analysis of HBr cell spectra made with the LINFIT v.8.2 algorithm (Hase et al., 1999). These cell spectra were recorded to characterize the instrumental line shape of the Jungfraujoch Bruker FTS. The SZA error impact on COF₂ retrievals has been deduced by assuming an accuracy of $\pm 0.2^\circ$ for zenith angles associated with each FTIR spectrum. This accuracy is compatible with the experimental observation conditions. To complete our error budget, the impact of two systematic error sources has also been evaluated: the shape of the COF₂ a priori vertical distribution and the uncertainty affecting the COF₂ line intensities. Their magnitudes have also been estimated through sensitivity tests. To quantify the impact of the COF₂ a priori VMR profile on COF₂ retrieved products we have used the same COF₂ a priori distribution derived by Mélen et al. (1998) from the ATMOS/SL3 1985 experiment instead of the mean COF₂ VMR profile derived from ACE-FTS measurements that we have adopted in our FTIR analysis (described in the previous section). The shapes of these two profiles are slightly different. In particular, the COF₂ profile derived from ATMOS measurements peaks at higher altitude (close to 35 km). In practice, this 20-year old profile has also been horizontally scaled in order to obtain a more realistic COF₂ total column, close to the value deduced from the ACE-FTS profile. To quantify

the impact of the uncertainty in the COF₂ line intensities on our retrievals, we have modified the HITRAN 2004 spectroscopic line list in accordance with the intensity uncertainty indices reported in Table 5 of Rothman et al. (2005). For all COF₂ lines included in our InSb microwindows, these authors quote uncertainties on the line intensities of greater than 20%. For all COF₂ lines included in our MCT microwindows, the corresponding HITRAN 2004 indices indicate that intensity uncertainties are between 10 and 20%. We have thus included line intensities in our retrievals modified by 25% for the InSb domain, and by 15% for the MCT range.

For each spectral range, Table 3 provides contributions from each random or systematic error, listed above, on COF₂ total and 17–30 km partial columns. For each wavenumber region, these error values have been obtained by using representative subsets of FTIR spectra covering various observational and fitting conditions (SZA range, spectral resolution, period of the year, time of the day, number of spectra combined during the multi-spectrum fit approach). When taking into account the six error sources presented in Table 3, the total random error affecting our COF₂ retrieved total columns is close to 10% for both spectral ranges. For the COF₂ 17–30 km partial columns, the total random error is a little higher, with values around 12% and 15% for InSb and MCT regions, respectively. Considering the very weak absorptions of COF₂ in our selected microwindows, the precision obtained for carbonyl fluoride column values with the multi-spectrum approach is very good: for comparison, the retrieval approach used by Mélen et al. (1998) reported a total random error of 23% in the COF₂ total columns. The situation is not so good for systematic errors: the high error values observed are mainly due to large uncertainties of up to 30% in the COF₂ lines intensities in the InSb range. Mélen et al. (1998) reports a total systematic error affecting their COF₂ total column of 18%, with a spectroscopic uncertainty of only 10%. However, this value seems a rather optimistic, since no major updates for COF₂ lines intensities (and their corresponding uncertainties) in the ν_1 band have occurred between the 1996 and 2004 versions of HITRAN line list (see also the end of the next section). Finally, for each random or systematic error source discussed, corresponding vertical distributions are very similar in both spectral domains, with peak values always observed within the FTIR sensitivity range.

4 Discussion of line parameters and retrieval approach

We have shown in the previous section that the multi-spectrum retrieval approach is the most sensitive to COF₂ between 17 and 30 km, with the largest fraction of the retrieved information always coming from the measurement. Using a simple example, we will further demonstrate that this sensitivity is also sufficient to distinguish between different air mass types, such as polar and midlatitude air masses. The

Table 3. Major random and systematic error sources and resulting relative uncertainties (%) affecting COF₂ total and [17–30] km partial columns derived from InSb and MCT spectral ranges. For both domains, these values have been obtained by using the multi-microwindow multi-spectrum approach running with a representative subset of the whole FTIR database analyzed in this study (see text for details).

Error source	Error on COF ₂ total column (%)		Error on COF ₂ [17–30] km partial column (%)	
Random errors				
	InSb	MCT	InSb	MCT
Smoothing error	4.8	8.5	7.9	11.1
Measurement error	6.4	7.5	8.1	9.6
Model parameter error	0.5	0.5	0.5	0.5
NCEP T profiles	0.4	2.5	0.8	2.2
ILS	1.3	2.4	1.5	2.8
SZA	1.2	1.8	1.5	2.1
TOTAL	8.2	12.0	11.5	15.3
Systematic errors				
	InSb	MCT	InSb	MCT
COF ₂ a priori VMR profile	0.8	1.9	5.2	7.0
COF ₂ line parameter uncertainties	27.9	12.9	34.4	15.8
TOTAL	28.7	14.8	39.6	22.8

top panel of Fig. 4 shows the evolution of the polar vortex for the last seven days of January 2005 over Western Europe. The Jungfraujoch station is identified by a white circle on each map. Potential vorticity (PV) maps over Europe used here are provided by the European Center for Medium range Weather Forecasting (ECMWF; see <http://www.ecmwf.int/>). The potential temperature level of these maps (475 K, which corresponds to an altitude of about 20 km) is the level generally used to follow polar airmasses. As the edge of the vortex (characterized by higher PV values – see colored legend of PV maps on the right part of Fig. 4) passes over the Jungfraujoch site on 27 January, enhancement in stratospheric COF₂ VMR is observed in the corresponding carbonyl fluoride profile retrieved from ISSJ spectra by using both sets of microwindows and the multi-spectrum approach (lower panel of Fig. 4: left: InSb range; right: MCT range). As these polar airmasses, enriched in fluorine compounds, leave the Jungfraujoch region, the COF₂ VMR decreases to values more in line with typical values observed during this period of the year (for each daily COF₂ VMR profile presented on Fig. 4, corresponding 17–30 km partial column is also noted in the legend). Information content obtained from the multi-spectrum approach is sufficient to catch such special atmospheric events. We also see from Fig. 4 that the consistency (e.g. in terms of profile shape) between the COF₂ vertical profiles retrieved from both wavenumber regions is very good.

We have mentioned previously (Sect. 1) that a systematic bias of 6% was observed by Mélen et al. (1998) between COF₂ total columns independently derived from InSb and

MCT regions. However, this bias was not found by Notholt et al. (1995). In order to compare the behavior of our time series with these previous results, we have computed the relative differences between COF₂ profiles retrieved from InSb and MCT microwindows for the 215 common measurement days in each time series over the period studied. The result corresponding to the sensitivity range (from 17 to 30 km) is plotted in red in frame (A) of Fig. 5. Error bars correspond to a 1- σ standard deviation on the mean. Throughout the entire altitude range, we do not find any significant bias between the two data sets. In the sensitivity range, the relative mean difference has a maximum of around 12% in the lower stratosphere.

A similar agreement is found when comparing total and partial columns derived from both spectral ranges for the same set of all common days between January 2000 and December 2007. Relative mean differences computed as $[(\text{InSb}-\text{MCT})/\text{MCT}] \times 100$ for COF₂ 17–30 km partial columns (see frame (B) of Fig. 5) and for COF₂ total columns (see frame (C) of Fig. 5) are $0.3 \pm 7.3\%$ and $1.0 \pm 6.5\%$, respectively. In frames (B) and (C) of Fig. 5, the solid and dotted lines represent the mean value and 1- σ standard deviation on the mean, respectively. For the time period studied here, no significant bias has thus been observed between the COF₂ total columns derived from the InSb (ν_1) and the MCT (ν_4) bands, in agreement with Notholt et al. (1995), but contrary to Mélen et al. (1999). The COF₂ spectroscopic parameters used by Mélen et al. (1999) were from the 1996 version of the HITRAN line list (Rothman et al., 1998). In the present study, we have used the HITRAN 2004 edition,

as mentioned in Sect. 2. Table 4 compares the number of CO₂ lines available in the 1996 and 2004 versions of HITRAN, in the wavenumber limits of each set of microwindow used for our retrievals. The last column provides relative mean differences and 1- σ standard deviations observed for the CO₂ lines intensities, calculated as $[(\text{HIT04-HIT96})/\text{HIT96}] \times 100(\%)$. The number N of lines common to both compilations and used to compute relative mean differences is given in parentheses. For the InSb region, line width parameters for CO₂ are the same in the 1996 and 2004 versions of HITRAN. However, a major update occurred with the number of CO₂ lines increasing by almost a factor 2. Corresponding line intensities have also been revised by almost 3%. For all microwindows in the MCT range, the 1996 and 2004 versions of HITRAN are identical. However, these spectroscopic differences are not sufficient to completely explain the 6% bias observed by Mélen et al. (1999) between CO₂ total columns derived from the ν_1 and the ν_4 bands. For one year of observations at ISSJ (namely, 2005 for which the available number of suitable spectra is a maximum), we have compared CO₂ columns retrieved by using the two spectroscopic parameters sets: the change in spectroscopic parameters causes mean differences of only $1.4 \pm 3.0\%$ for CO₂ total columns, and of only $0.9 \pm 4.1\%$ for CO₂ 17–30 km partial columns. We may thus suppose that, in addition to the spectroscopic updates (for CO₂ and interfering gas lines in our microwindows), it is the retrieval procedure and the use of different input parameters (i.e., a priori CO₂ VMR profile and the sets and limits of microwindows selected for the retrievals) that is responsible of the better agreement between CO₂ abundances retrieved in the two spectral ranges.

5 Comparisons with model data

Our daily mean FTIR CO₂ 17–30 km partial columns have also been confronted with daily values specifically computed for the Jungfraujoch location using the KASIMA (Karlsruhe Simulation model of the Middle Atmosphere) and SLIMCAT models.

The KASIMA model used in this study is a global circulation model including stratospheric chemistry for the simulation of the behavior of physical and chemical processes in the middle atmosphere (Reddmann et al., 2001; Ruhnke et al., 1999). The meteorological component is based on a spectral architecture with the pressure altitude $z = -H \ln\left(\frac{p}{p_0}\right)$ as vertical coordinate where $H=7$ km is a constant atmospheric scale height, p is the pressure, and $p_0=1013.25$ hPa is a constant reference pressure. A horizontal resolution of T21 (about 5.6×5.6 degrees) has been used. In the vertical regime, 63 levels between 10 and 120 km pressure altitude and a 0.75 km spacing from 10 up to 22 km with an exponential increase above were used. The meteorology module of the KASIMA model consists of three versions: the diagnos-

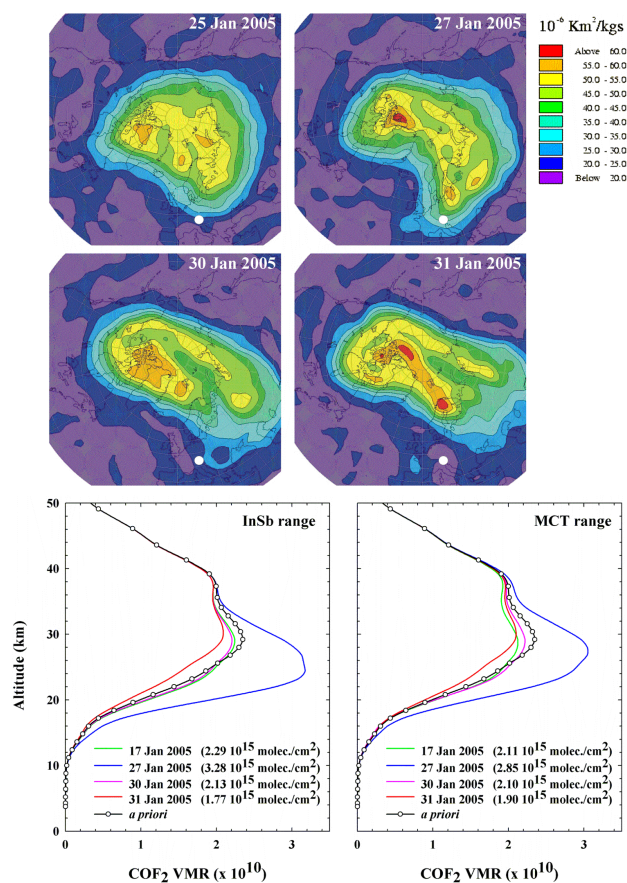


Fig. 4. Example of CO₂ vertical profiles derived by applying the multi-spectrum approach to FTIR ground-based observations performed at ISSJ during January 2005 (lower panel). The overpass, above the Jungfraujoch (white circle on ECMWF PV maps at 475 K level on top panel), of the edge of the vortex on January 27th is well captured by the FTIR measurements (low panel: left: CO₂ profiles derived from the InSb set of microwindows; right: CO₂ profiles derived from the MCT set of microwindows).

tic model, the prognostic model and the nudged model which combines the prognostic and diagnostic model (Kouker et al., 1999). In the version used here, the model is nudged towards the operational ECMWF analyses of temperature, vorticity and divergence between 18 and 48 km pressure altitude. Below 18 km, the meteorology is based on ECMWF analyses without nudging, above 48 km pressure altitude, the prognostic model has been used. The rate constants of the gas phase and heterogeneous reactions are taken from Sander et al. (2003). The photolysis rates are calculated online with the fast-j2 scheme of Bian and Prather (2002). The distributions of the chemical species in this model run were initialized on 30 April 1972, with data from a long-term KASIMA run.

The 3-D SLIMCAT CTM uses various data (including meteorological data such as winds and temperature, emission scenario of the source gases, chemistry schemes, etc.) to derive the atmospheric transport and to calculate abundances

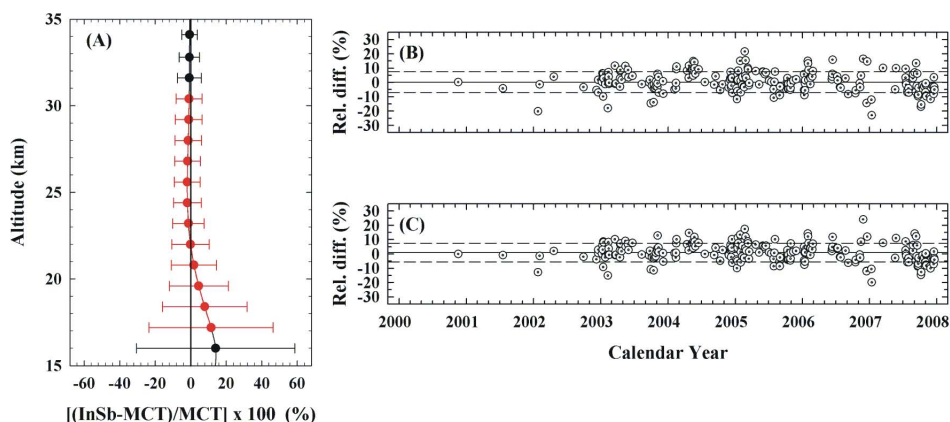


Fig. 5. Frame (A) relative mean differences (calculated as $[(\text{InSb}-\text{MCT})/\text{MCT}] \times 100$) between CO₂ vertical profiles retrieved from InSb and MCT spectral ranges using simultaneously a multi-microwindow and a multi-spectrum approach. The sensitivity range of the retrievals is plotted in red. Error bars indicate 1σ standard deviation around the mean; frame (B) relative mean differences between CO₂ [17–30] km partial columns derived from both spectral ranges for the 215 common measurement days of the January 2000–December 2007 time period; frame (C) relative mean differences between CO₂ total columns derived from both spectral ranges for the 215 common measurement days of the January 2000–December 2007 time period. In frames (B) and (C), solid and dashed lines represent the mean value and 1σ standard deviation around the mean, respectively.

Table 4. Number of CO₂ lines in each InSb and MCT microwindow, as listed in the HITRAN 1996 (second column) and HITRAN 2004 (third column) spectroscopic line lists. The 2004 version has been used in this study while the work by Mélen et al. (1999) was based on the 1996 compilation. The last column provides mean relative differences and 1σ standard deviations observed on the line intensities (calculated as $[(\text{HIT04}-\text{HIT96})/\text{HIT96}] \times 100$). The number N of lines common to both compilations and used to compute relative mean differences is given in parentheses. No updates have been observed for CO₂ lines located in the MCT range.

Microwindow limits (cm ⁻¹)	# CO ₂ lines (HIT-1996)	# CO ₂ lines (HIT-2004)	Intensity relative differences (N)
InSb range			
1936.15–1936.34	52	80	2.80±0.02 (52)
1951.89–1952.05	23	42	2.80±0.02 (23)
1952.62–1952.78	23	42	2.80±0.02 (23)
MCT range			
1230.75–1231.20	136	136	0.00±0.00 (136)
1233.90–1234.20	96	96	0.00±0.00 (96)
1234.35–1234.63	86	86	0.00±0.00 (86)

of tropospheric and stratospheric gases. The first description of SLIMCAT appears in Chipperfield et al. (1993). During the last years, the SLIMCAT runs have already been exploited to perform comparisons of fluorine species abundances with satellite and ground-based observations (Chipperfield et al., 1997). More recently, it has also been used to derive long-term trends of atmospheric compounds (Feng et al., 2007). All information concerning the SLIMCAT model version used in this work can be found in Chipperfield (2006) or on the SLIMCAT website (see <http://www.env.leeds.ac.uk/slimcat>).

As we have shown in the previous section that there is no significant difference between InSb and MCT retrieved CO₂ partial columns, the InSb and MCT datasets have been merged to obtain a denser FTIR time series, more appropriate for trend studies and for comparisons with model or experimental datasets. So, between January 2000 and December 2007, there are 475 days available for direct comparisons with daily KASIMA and SLIMCAT simulations. As KASIMA and SLIMCAT models use ECMWF analyses to force their meteorology, their CO₂ VMR profiles have been converted into partial columns using pressure and temperature profiles from ECMWF operational analyses.

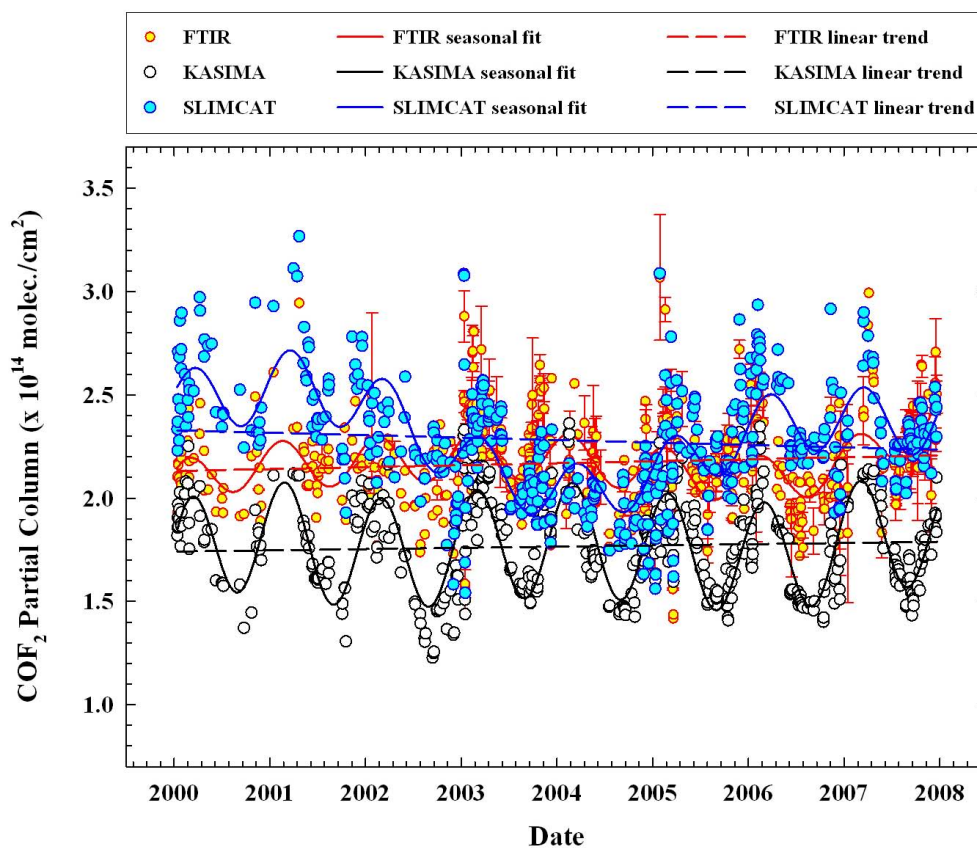


Fig. 6. COF₂ 17–30 km partial column time series as observed by the FTIR instrument operated at the Jungfraujoch station (yellow dots) and as computed by the KASIMA and SLIMCAT 3-D CTM models (white and blue dots, respectively). Solid lines reproduce seasonal variations adjusted for each data set while dashed lines correspond to a linear trend for the de-seasonalized time series.

Figure 6 plots the merged FTIR time series with coincident KASIMA and SLIMCAT data. For the Jungfraujoch time series, error bars reproduce one mean standard deviation; FTIR data points without error bars correspond to days with only one measurement. It clearly appears from Fig. 6 that a significant perturbation affects the middle of the SLIMCAT time series. This could be explained by the fact that the ECMWF meteorological analyses used by the SLIMCAT model are not an homogeneous set, as ECMWF has changed their vertical resolution several times. These changes cover three time periods, namely January 2000–December 2001, January 2002–January 2006 and February 2006–onwards and cause a decrease in the SLIMCAT COF₂ columns from 2002 to 2006. However, the KASIMA time series is not affected by these changes in ECMWF vertical resolution as the calculation of the vertical velocities is different compared to SLIMCAT and as the ECMWF data are nudged to the KASIMA model environment in order to yield a realistic age of air (Reddmann et al., 2001). Furthermore, although the KASIMA time series seems to be able to reproduce special events (linked for example to particular air mass conditions), one can see in Fig. 6 that the KASIMA variability is significantly less than in the

other two time series. Seasonal variations and trends in each data set have been fitted with a function $C(t)$ that combines a polynomial of degree n $C_n(t)$ and a cosine term, $C_{\cos}(t)$:

$$C_n(t) = c_0 + c_1(t - t_0) + c_2(t - t_0)^2 + \dots + c_n(t - t_0)^n \quad (1)$$

$$C_{\cos}(t) = A \cos(2\pi(t - t_0) - t_1) \quad (2)$$

$$C(t) = C_n(t)[1 + C_{\cos}(t)] \quad (3)$$

where c_0 is the COF₂ partial column at an arbitrary reference time t_0 (taken as 2000, the beginning of the time period studied). A is the relative amplitude of the seasonal variation and t_1 is the fraction of the calendar year corresponding to the seasonal maximum. Results of such fits are represented by solid lines in Fig. 6. For each time series, the best agreements are obtained (on the basis of correlation coefficient values) when using a polynomial function of order 6 in Eq. (1). Seasonal variations are well captured in each case. Table 5 summarizes the fitted values of the main parameters appearing in Eq. (2), that characterize the seasonal variations of each time series. With a value close to 15%, the relative amplitude of the seasonal variation in the KASIMA

Table 5. Main seasonal characteristics of the time series fits presented in Fig. 6. For each data set, second column (*A*) provides relative amplitude of the seasonal variation while third column (*t*₁) gives the time (expressed in fractional calendar year units) when the cosine component of each fit reaches its maximum value. This time is converted into calendar days in the last column.

Data set	<i>A</i> (%)	<i>t</i> ₁	<i>t</i> ₁
FTIR	5.30	0.13	16 February
KASIMA	15.42	0.16	27 February
SLIMCAT	6.62	0.21	18 March

data set is more than twice the values obtained from the other two time series (5 and 6%, for FTIR and SLIMCAT, respectively). We have compared these values to the one published by Mélen et al. (1998). The fitting approach used by Mélen et al. (1998) is based on two microwindows located in the ν_1 band and fitted separately during the retrieval procedure. For the 10-year time period (1985–1995) covered in that paper, Mélen et al. found a mean amplitude of about 9% for the seasonal cycle, i.e. just in the middle of the amplitude ranges deduced from the present study. For the phase of the seasonal cycle, the FTIR and KASIMA data give COF₂ maximum values between mid- and end of February while the SLIMCAT model predicts maximum values in the second part of March (Table 5). From these results, it can be seen that the maximum COF₂ abundances occur during or at the end of winter, when photodissociation processes are at their minimum, while the minimum COF₂ concentrations occur in late summer. Mélen et al. (1998) have deduced a seasonal maximum value equal to 0.17 (in fractional calendar year units), which corresponds to the 3 March.

To estimate linear trends (reproduced with dashed lines in Fig. 6), the seasonal variations of each time series have been removed. Linear trends for the time period 2000–2007 are 3.5 ± 1.8 % and 2.7 ± 1.5 % for the FTIR and KASIMA time series, respectively. This corresponds to linear COF₂ increases of 0.4 ± 0.2 %/year and 0.3 ± 0.2 %/year, for FTIR and KASIMA data sets, respectively. A negative trend of -4.0 ± 1.9 % (or -0.5 ± 0.2 %/year) is found from the SLIMCAT time series. This is probably a consequence of the discontinuity in the meteorological data used by the SLIMCAT model, as already described above.

Linear COF₂ trends deduced from the present study are considerably lower than the value found by Mélen et al. (1998) 10 years ago, who observed an average COF₂ linear trend equal to 4.0 ± 0.5 %/year for the 1985–1995 time period. This slowing down of this COF₂ linear trend, between 1985–1995 and 2000–2007, results from the phase out of its principal source gases (CFC-12 and CFC-11). Figure 1–1 of the WMO report (2007) shows the trends for these two species during the 1980–2005 time period. Data re-

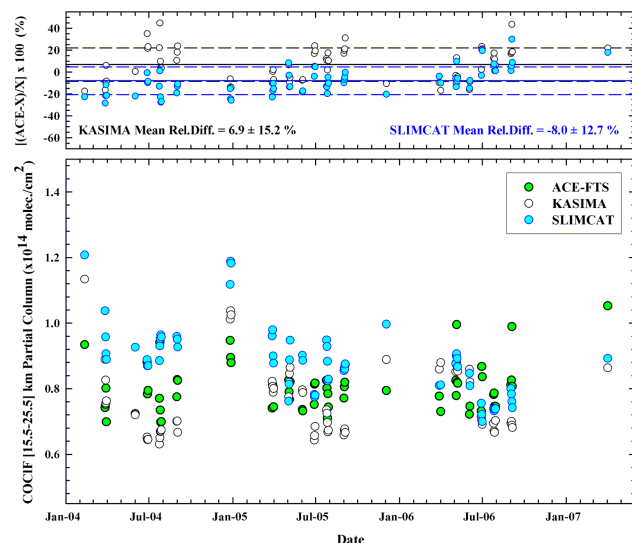


Fig. 7. COCIF [15.5–25.5] km partial columns time series as observed by the ACE-FTS space instrument (green dots) and as computed by the KASIMA and SLIMCAT 3-D CTM models (white and light blue dots, respectively). Top panel reproduces relative differences between ACE-FTS data and model data (solid line: mean relative difference; dotted lines: 1σ standard deviation on the mean).

produced in that figure are those provided by the Advanced Global Atmospheric Gases Experiment (AGAGE) network (Prinn et al., 2000), as well as by the National Oceanic and Atmospheric Administration/Earth System Research Laboratory (NOAA/ESRL – Montzka et al., 1999; Thompson et al., 2004) and the University of California at Irvine (UCI – Blake et al., 1996; Blake et al., 2001). A small but obvious decrease in the abundance of CFC-11 is observed since the middle of the nineties, and the rate of growth of CFC-12 has slowed down since the end of the nineties. Table 1–2 of WMO (2007) also reports a grow rate of the CFC-11 mole fraction (expressed in ppt) of around -0.7 %/year, for the 2003–2004 time period; the corresponding values published for CFC-12 are inconsistent: while AGAGE measurements give a slight decrease of 0.1 %/year, an increase of 0.3 %/year results from UCI analysis. No trend is observed from NOAA data. In addition, the annual changes in the CFC-12 vertical abundance above central Europe and from 1987 to 2005 can be also found in Zander et al. (2005); these authors report a decrease of 0.16 %/year in the CFC-12 vertical total column (in molec./cm²) for the 2003–2004 time period. Whatever the CFC-12 trend value, a stabilization of the CFC-12 mole fraction at around 540 ppt between 2003 and 2005 is clearly visible in Fig. 1–1 of WMO (2007). Until now, the decrease or the stabilization observed for these two major fluorine-containing source gases (CFC-12 and CFC-11) has only been partially compensated for by increases in CFC substitutes (such as HCFC-22 and HCFC-134a), so that a slowdown of the increase in total inorganic fluorine F_y is

observed (Figs. 1–19 of WMO, 2007). Decreases observed in the CO₂ rates derived from FTIR and KASIMA time series presented in this study are a direct consequence of these changes.

While FTIR and SLIMCAT data sets do not show significant relative differences (mean relative difference computed over 17–30 km partial columns as [(FTIR-SLIMCAT)/SLIMCAT]×100 is $-3.5\pm 10.6\%$), it is obvious from Fig. 6 that a large bias (around 25%) exists between the FTIR and KASIMA. Two main possibilities could explain this KASIMA underestimation. The first one is that KASIMA uses the wrong CO₂ VMR values at its lowest altitude level (i.e. 7 km). This could cause biased CO₂ abundances in the upper troposphere / lower stratosphere (UTLS). The second possibility is that the KASIMA partitioning between fluorine species (i.e. HF, CO₂ and COClF) could be erroneous. As we have shown previously (Sect. 3) that FTIR retrievals have no sensitivity to CO₂ below 17 km, it is not possible to directly compare FTIR and KASIMA CO₂ UTLS partial columns, to check the validity of the first hypothesis. However, as previous comparisons have demonstrated the good agreement between FTIR and KASIMA abundances for HF (Ruhnke et al., 2007), we thus have compared COClF partial columns computed by the KASIMA model with ACE-FTS satellite data in order to check on the validity of the second hypothesis (Fig. 7). Satellite data are well suited for this exercise (Rinsland et al., 2007; Fu et al., 2009) as water vapor interferences make the detection of COClF from FTIR ground-based spectra difficult. Only ACE-FTS occultations located in the 40–50° N latitude band have been compared with KASIMA data, which represents a set of 64 coincident points. Partial column limits (15–25 km) used are representative of the altitude range where the ACE-FTS instrument is able to record COClF vertical profiles. The top panel of Fig. 7 plots relative differences for the two time series. The mean relative difference value ($6.9\pm 15.2\%$) indicates that there is no significant bias between the data sets and thus suggests that the second hypothesis mentioned above should be rejected. Moreover, very recent redesign of the KASIMA chemistry module has indicated that the lower boundary value of CO₂ within the troposphere indeed significantly affects KASIMA CO₂ total columns. For the 64 coincident days evoked above, corresponding COClF partial columns computed by the SLIMCAT model are also reproduced on Fig. 7 (light blue dots). As for the KASIMA time series, no significant bias with respect to the ACE-FTS data is observed, confirming the good agreement existing for COClF between model calculations and satellite measurements.

6 Conclusions and perspectives

This paper describes the advantages of using a new approach to invert CO₂ vertical distributions from ground-based FTIR solar spectra. The idea is to combine data

from several spectral microwindows and all available spectra, recorded at the same resolution during the same day, in the retrievals in order to increase the information content. We have selected two sets of three microwindows, located either in the ν_1 or in the ν_4 CO₂ absorption bands, and have demonstrated that there is a gain in information content in this multi-microwindows multi-spectrum fitting strategy. In each case, a significant improvement in DOFS and first eigenvalues is obtained, allowing us to derive one CO₂ partial column between 17 and 30 km. Mean DOFS values computed for the January 2000–December 2007 time period are 1.23 ± 0.17 and 1.16 ± 0.30 for InSb (2–5.5 μm) and MCT (7–14 μm) regions, respectively. In all cases, the largest fraction of the information comes from the measurement rather than the a priori. We have also shown that the information content in the multi-spectrum approach is sufficient to observe special atmospheric events, such as polar vortex overpasses. In the ν_4 region, total random errors affecting CO₂ 17–30 km partial columns and CO₂ total columns are close to 12% and 8%, respectively. In the ν_1 region, the corresponding values are 15% and 12%. For both spectral ranges, the highest systematic total errors have been observed (ranging from 15% to 40%), mainly due to high uncertainties characterizing CO₂ lines intensities reported in the HITRAN 2004 database. Comparisons of CO₂ vertical profiles retrieved between 17 and 30 km as well as corresponding partial columns derived from both spectral ranges do not show any significant bias. The same conclusion can be made for total columns. This latter result is in agreement with results from Notholt et al. (1995) but is not consistent with the systematic 6% mean bias observed between CO₂ total columns derived from the ν_1 and the ν_4 absorption bands by Mélen et al. (1999). This difference in behavior between our results and those obtained by Mélen et al. (1999) cannot be attributed totally to the difference in spectroscopic parameters used for the retrievals. It seems that a different choice of input parameters and the multi-microwindow multi-spectrum procedure leads to a better agreement between CO₂ columns derived from the ν_1 and the ν_4 absorption bands.

Comparisons of the merged FTIR data set (i.e. obtained by averaging CO₂ data coming from ν_1 and ν_4 bands) with CO₂ 17–30 km partial columns generated by the KASIMA and SLIMCAT 3-D CTMs has also been presented. We did not notice any significant bias between the FTIR and SLIMCAT time series. However, a significant bias of about 25% has been observed between the FTIR and KASIMA data sets, with KASIMA giving lower CO₂ 17–30 km partial columns. It seems that this bias could be attributed to incorrect lower boundary conditions used in the KASIMA model. Linear trends over the 2000–2007 time period as well as the main seasonal variation parameters have also been derived for each time series. Except for the SLIMCAT time series, very low CO₂ growth rates have been derived from FTIR and KASIMA time series

($0.4 \pm 0.2\%$ /year and $0.3 \pm 0.2\%$ /year, respectively). A negative trend ($-0.5 \pm 0.0\%$ /year) has been obtained from the SLIMCAT data set. However, this is probably due to discontinuities in the ECMWF data, which significantly decreases COF₂ SLIMCAT columns from 2002 to 2006. Decreases in the COF₂ growth rate can be mainly attributed to the stabilization of the CFC-12 tropospheric concentration and to the recent decrease observed in the CFC-11 atmospheric abundance.

Finally, the three time series all display the COF₂ seasonal cycle. The relative amplitudes range from 5 to 15%, with a seasonal maximum between mid-February and the end of March. These seasonal cycle results agree quite reasonably with the previous study by Mélen et al. (1998). However, it should be kept in mind that the time periods under investigations are not the same. In the future, it would be interesting to use the multi-microwindow multi-spectrum approach at other ground-based FTIR stations. This will serve to demonstrate the effectiveness of this fitting procedure and to increase the coverage of ground-based COF₂ measurements. This could be used to extend this study of COF₂ seasonal and latitudinal variability as well as the long-term trend at different sites. In addition, the use of a multi-microwindow multi-spectrum fitting procedure could increase the vertical information content for other atmospheric gases that have weak signatures in FTIR solar spectra.

Acknowledgements. We would like to thank the International Foundation High Altitude Research Stations Jungfraujoch and Gornergrat (HFSJG, Bern) and the University of Liège for supporting the facilities needed to perform the observations and their analyses. University of Liège work is supported primarily by the Belgian Federal Science Policy Office. Financial support by projects Prodex-ACE and SECPEA as well as GEOMON is further acknowledged. Thanks are also extended to all collaborators having contributed to the observations at the Jungfraujoch. The Atmospheric Chemistry Experiment (ACE), also known as SCISAT, is a Canadian-led mission mainly supported by the Canadian Space Agency and the Natural Sciences and Engineering Research Council of Canada. The authors also thank the ECMWF for providing the PV maps used in this work.

Edited by: M. van Roozendael

References

- Bernath, P. F., McElroy, C. T., Abrams, M. C., et al.: Atmospheric Chemistry Experiment (ACE): mission overview, *Geophys. Res. Lett.*, 32, L15S01, doi:10.1029/2005GL022386, 2005.
- Bian, H. and Prather, M. J.: Fast-J2: Accurate simulation of stratospheric photolysis in global chemical models, *J. Atmos. Chem.*, 41, 281–296, 2002.
- Blake, D. R., Chen, T.-Y., Smith Jr., T. W., Wang, C. J.-L., Wingen, O. W., Blake, N. J., Rowland, F. S., and Mayer, E. W.: Three-dimensional distribution of non-methane hydrocarbons and halocarbons over the northwest Pacific during the 1991 Pacific Exploratory Mission (PEM-West A), *J. Geophys. Res.*, 101, 1763–1778, 1996.
- Blake, N. J., Blake, D. R., Simpson, I. J., Lopez, J. P., Johnston, N. A. C., Swanson, A. L., Katzenstein, A. S., Meinardi, S., Sive, B. C., Colman, J. J., Atlas, E., Flocke, F., Vay, S. A., Avery, M. A., and Rowland, F. S.: Large-scale latitudinal and vertical distributions of NMHCs and selected halocarbons in the troposphere over the Pacific Ocean during the March–April 1999 Pacific Exploratory Mission (PEM-Tropics B), *J. Geophys. Res.*, 106, 32627–32644, 2001.
- Ceccherini, S.: Analytical determination of the regularization parameter in the retrieval of atmospheric vertical profiles, *Opt. Lett.*, 30, 2554–2556, 2005.
- Connor, B. J., Parrish, A., Tsou, J.-J., and McCormick, P.: Error analysis of the ground-based microwave ozone measurements during STOIC, *J. Geophys. Res.*, 100, 9283–9291, 1995.
- Chipperfield, M. P., Cariolle, D., Simon, P., Ramaroson, R., Lary, D. J.: A 3-dimensional modeling study of trace species in the Arctic lower stratosphere during winter 1989–1990, *J. Geophys. Res.*, 98, 7199–7218, 1993.
- Chipperfield, M. P., Burton, M., Bell, W., Paton Walsh, C., Blumenstock, T., Coffey, M. T., Hannigan, J. W., Mankin, W. G., Galle, B., Mellqvist, J., Mahieu, E., Zander, R., Notholt, J., Sen B., and Toon, G. C.: On the use of HF as a reference for the comparison of stratospheric observations and models, *J. Geophys. Res.*, 102, 12901–12919, 1997.
- Chipperfield, M. P.: New version of the TOMCAT/SLIMCAT offline Chemical Transport Model: intercomparison of stratospheric tracer experiments, *Q. J. R. Meteorol. Soc.*, 132, 1179–1203, 2006.
- Feng, W., Chipperfield, M. P., Dorf, M., Pfeilsticker, K., and Ricaud, P.: Mid-latitude ozone changes: studies with a 3-D CTM forced by ERA-40 analyses, *Atmos. Chem. Phys.*, 7, 2357–2369, 2007, <http://www.atmos-chem-phys.net/7/2357/2007/>.
- Fu, D., Boone, C. D., Bernath, P. F., Weisenstein, D. K., Rinsland, C. P., Manney G. L., and Walker, K. A.: First global observations of atmospheric COClF from the Atmospheric Chemistry Experiment mission, *J. Quant. Spec. and Rad. Transf.*, 110, 974–985, 2009.
- Hase, F., Blumenstock, T., and Paton-Walsh, C.: Analysis of instrumental line shape of high-resolution FTIR-spectrometers using gas cell measurements and a new retrieval software, *Appl. Opt.*, 3417–3422, 1999.
- Kaye, J. A., Douglas, A. R., Jackman, C. H., Stolarski, R. S., Zander, R., and Roland, G.: Two-dimensional model calculation of fluorine-containing reservoirs species, *J. Geophys. Res.*, 96, 12865–12881, 1991.
- Ko, M. K. W., Sze, N. D., and Weisenstein, D. K.: The roles of dynamical and chemical processes in determining the stratospheric concentration of ozone in one-dimensional and two-dimensional models, *J. Geophys. Res.*, 94, 9889–9896, 1989.
- Kouker, W., Langbein, I., Reddmann T., and Ruhnke, R.: The Karlsruhe Simulation Model of the Middle Atmosphere (KASIMA), Version 2, FZK Report 6278, Forschungszentrum Karlsruhe, Germany, 1999.
- Mélen, F., Mahieu, E., Zander, R., Rinsland, C. P., Demoulin, P., Roland, G., Delbouille, L., and Servais, C.: Vertical column abundances of COF₂ above the Jungfraujoch Station, derived from ground-based infrared solar observations, *J. Atmos. Chem.*, 29,

- 119–134, 1998.
- Mélen, F., Mahieu, E., Demoulin, P., Servais, C., and Zander, R.: Vertical column abundances of COF₂ above the Jungfraujoch Station: update and consolidation of the database with measurements in the ν₄ band region, in Proceedings of Atmospheric Spectroscopy Applications 1999, Reims, France, 1–3 September, 1999.
- Montzka, S. A., Butler, J. H., Elkins, J. W., Thompson, T. M., Clarke, A. D., and Lock, L. T.: Present and future trends in the atmospheric burden of ozone-depleting halogens, *Nature*, 398, 690–694, 1999.
- Nassar, R., Bernath, P. F., Boone, C. D., McLeod, S. D., Skelton, R., Walker, K. A., Rinsland, C. P., and Duchatelet, P.: A global inventory of stratospheric fluorine in 2004 on Atmospheric Chemistry Experiment Fourier transform spectrometer (ACE-FTS) measurements, *J. Geophys. Res.*, 111, D22313, doi:10.1029/2006JD007395, 2006.
- Notholt, J., Meier, A., and Peil, S.: Total column densities of tropospheric and stratospheric trace gases in the undisturbed arctic summer atmosphere, *J. Atmos. Chem.*, 20, 311–332, 1995.
- Pougatchev, N. S. and Rinsland, C. P.: Spectroscopic study of the seasonal variation of carbon monoxide vertical distribution above Kitt Peak, *J. Geophys. Res.*, 100, 1409–1416, 1995.
- Pougatchev, N. S., Connor, B. J., and Rinsland, C. P.: Infrared measurements of the ozone vertical distribution above Kitt Peak, *J. Geophys. Res.*, 100, 16689–16697, 1995.
- Prinn, R. G., Weiss, R. F., Fraser, P. J., Simmonds, P. G., Cunnold, D. M., Alyea, F. N., O'Doherty, S., Salameh, P., Miller, B. R., Huang, J., Wang, R. H. J., Hartley, D. E., Harth, C., Steele, L. P., Sturrock, G., Midgley, P. M., and McCulloch, A.: A history of chemically and radiatively important gases in air deduced from ALE/GAGE/AGAGE, *J. Geophys. Res.*, 105, 17751–17792, 2000.
- Reddmann, T., Ruhnke, R., and Kouker, W.: Three-dimensional model simulations of SF₆ with mesospheric chemistry, *J. Geophys. Res.*, 106, 14525–14537, 2001.
- Reisinger, A. R., Jones, N. B., Matthews, W. A., and Rinsland, C. P.: Southern hemisphere ground based measurements of carbonyl fluoride (COF₂) and hydrogen fluoride (HF): partitioning between fluoride reservoir species, *Geophys. Res. Lett.*, 21, 797–800, 1994.
- Rinsland, C. P., Zander, R., Brown, L. R., Farmer, C. B., Park, J. H., Norton, R. H., Russell, III, J. M., and Raper, O. F.: Detection of carbonyl fluoride in the stratosphere, *Geophys. Res. Lett.*, 13, 769–772, 1986.
- Rinsland, C. P., Levine, J. S., Goldman, A., Sze, N. D., Ko, M. K. W., and Johnson, D. W.: Infrared measurements of HF and HCl total column abundances above Kitt Peak, 1997–1990: seasonal cycles, long-term increases and comparisons with model calculations, *J. Geophys. Res.*, 96, 15523–15540, 1991.
- Rinsland, C. P., Jones, N. B., Connor, B. J., Logan, J. A., Pougatchev, N. S., Goldman, A., Murcray, F. J., Stephen, T. M., Pine, A. S., Zander, R., Mahieu, E., and Demoulin, P.: Northern and southern hemisphere ground-based infrared measurements of tropospheric carbon monoxide and ethane, *J. Geophys. Res.*, 103, 28197–28218, 1998.
- Rinsland, C. P., Nassar, R., Boone, C. D., Bernath, P., Chiou, L., Weisenstein, D. K., Mahieu, E., and Zander, R.: Spectroscopic detection of COClF in the tropical and mid-latitude lower stratosphere, *J. Quant. Spec. and Rad. Transf.*, 105, 467–475, 2007.
- Rodgers, C. D.: Inverse methods for atmospheric sounding: Theory and Practice, Volume 2 of Series on Atmospheric, Oceanic and Planetary Physics, World Scientific Co. Pte. Ltd., 2000.
- Rothman, L. S., Rinsland, C. P., Goldman, A., Massie, S. T., Edwards, D. P., Flaud, J.-M., Perrin, A., Camy-Peyret, C., Dana, V., Mandin, J.-Y., Schroeder, J., McCann, A., Gamache, R. R., Wattson, R. B., Yoshino, K., Chance, K. V., Jucks, K. W., Brown, L. R., Nemtchinov, V., and Varanasi, P.: The HITRAN molecular spectroscopic database and HAWKS (HITRAN Atmospheric Workstation): 1996 edition, *J. Quant. Spec. and Rad. Transf.*, 60, 665–710, 1998.
- Rothman, L. S., Jacquemart, D., Barbe, A., Chris Benner, D., Birk, M., Brown, L. R., Carleer, M. R., Chackerian, Jr., C., Chance, K., Coudert, L. H., Dana, V., Devi, V. M., Flaud, J.-M., Gamache, R. R., Goldman, A., Hartmann, J.-M., Jucks, K. W., Maki, A. G., Mandin, J.-Y., Massie, S. T., Orphal, J., Perrin, A., Rinsland, C. P., Smith, M. A. H., Tennyson, J., Tolchenov, R. N., Toth, R. A., Vander Auwera, J., Varanasi, P., and Wagner, G.: The HITRAN 2004 molecular spectroscopic database, *J. Quant. Spec. and Rad. Transf.*, 96, 139–204, 2005.
- Ruhnke, R., Kouker, W., and Reddmann, T.: The influence of the OH + NO₂ + M reaction on the NO_y partitioning in the late arctic winter 1992/1993 as studied with KASIMA, *J. Geophys. Res.*, 104, 3755–3772, 1999.
- Ruhnke, R., Blumenstock, T., Duchatelet, P., Hamann, K., Hase, F., Kouker, W., Kramer, I., Mahieu, E., Mikuteit, S., Notholt, J., Reddmann, T., Schneider, M., Sinnhuber, B.-M., Sussmann, R., Velasco, V., Warneke, T., and Wiehle, M.: Measured and modelled trends of stratospheric Cl_y and F_y column amounts in the Northern Hemisphere, *Geophys. Res. Abstr.*, 9, 07597, 2007.
- Sander, S. P., Friedl, R. R., Ravishankara, A. R., Golden, D. M., Kolb, C. E., Kurylo, M. J., Huie, R. E., Orkin, V. L., Molina, M. J., Moortgat, G. K., and Finlayson-Pitts, B. J.: Chemical kinetics and photochemical data for use in atmospheric studies, Evaluation Number 14, JPL Publication 2–25 February, 2003.
- Sen, B., Toon, G. C., Blavier, J.-F., Fleming, E. L., and Jackman, C. H.: Balloon-borne observations of midlatitude fluorine abundance, *J. Geophys. Res.*, 101, 9045–9054, 1996.
- Steck, T.: Methods for determining regularization for atmospheric retrieval problems, *Appl. Opt.*, 41, 1788–1797, 2002.
- Thompson, T. M., Butler, J. H., Daube, B. C., Dutton, G. S., Elkins, J. W., Hall, B. D., Hurst, D. F., King, D. B., Kline, E. S., LaFleur, B. G., Lind, J., Lovitz, S., Mondeel, D. J., Montzka, S. A., Moore, F. L., Nance, J. D., Neu, J. L., Romashkin, P. A., Scheffer, A., and Snible, W. J.: Halocarbons and other atmospheric trace species, Section 5, in: Climate Monitoring and Diagnostics Laboratory: Summary Report No. 27, 2002–2003, edited by: Schnell, R., Buggle, A.-M., and Rosson, R., 115–135, NOAA/Climate Monitoring and Diagnostics Laboratory, Boulder, Colo., 2004.
- Walker, K. A., Cooper, M. D., Weigum, N., et al.: Global zonal mean distribution of carbonyl fluoride (COF₂), in preparation, 2009.
- Wilson, S. R., Schuster, G., and Helas, G.: Measurements of COFCl and CCl₂O near the tropopause, in: Ozone in the Atmosphere, edited by: Bojkov, R. D. and Fabian, P., A. Deepak Publisher, 302–305, 1989.

- WMO Report No. 50: Scientific Assessment of Ozone Depletion: 2006, World Meteorological Organization, P.O. Box 2300, Geneva 2, CH 1211, Switzerland, 2007.
- Zander, R., Rinsland, C. P., Mahieu, E., Gunson, M. R., Farmer, C. B., Abrams, M. C., and Ko, M. K. W.: Increase of carbonyl fluoride (COF₂) in the stratosphere and its contribution to the 1992 budget of inorganic fluorine in the upper stratosphere, *J. Geophys. Res.*, 99, 16737–16743, 1994.
- Zander, R., Mahieu, E., Demoulin, P., Duchatelet, P., Servais, C., Roland, G., Delbouille, L., De Mazière, M., and Rinsland, C. P.: Evolution of a dozen non-CO₂ greenhouse gases above Central Europe since the mid-1980s, *Environ. Sci.*, 2(2–3), 295–303 2005.